

Accelerating Discovery of Novel and Bioactive Ligands With Pharmacophore-Informed Generative Models

**Weixin Xie^{1,†}, Jianhang Zhang^{2,†}, Qin Xie², Chaojun Gong², Youjun Xu^{2,*},
Luhua Lai^{1,3,*}, and Jianfeng Pei^{1,*}**

¹Center for Quantitative Biology, Academy for Advanced Interdisciplinary Studies, Peking University, Beijing, China, 100871

²Infinite Intelligence Pharma, Beijing, China, 100083

³BNLMS, Peking-Tsinghua Center for Life Sciences at the College of Chemistry and Molecular Engineering, Peking University, Beijing, China, 100871

[†]Equal contribution

*Corresponding authors: xuyj@iipharma.cn, lhlai@pku.edu.cn, jfpei@pku.edu.cn

Abstract

Deep generative models have gained significant advancements to accelerate drug discovery by generating bioactive chemicals against desired targets. Nevertheless, most generated compounds that have been validated for potent bioactivity often exhibit structural novelty levels that fall short of satisfaction, thereby providing limited inspiration to human medicinal chemists. The challenge faced by generative models lies in their ability to produce compounds that are both bioactive and novel, rather than merely making minor modifications to known actives present in the training set. Recognizing the utility of pharmacophores in facilitating scaffold hopping, we developed TransPharmer, an innovative generative model that integrates ligand-based interpretable pharmacophore fingerprints with generative pre-training transformer (GPT) for *de novo* molecule generation. TransPharmer demonstrates superior performance across tasks involving unconditioned distribution learning, *de novo* generation and scaffold elaboration under pharmacophoric constraints. Its distinct exploration mode within the local chemical space renders it particularly useful for scaffold hopping, producing compounds that are structurally novel while pharmaceutically related. The efficacy of TransPharmer is validated through two case studies involving the dopamine receptor D2 (DRD2) and polo-like kinase 1 (PLK1). Notably in the case of PLK1, three out of four synthesized designed compounds exhibit

submicromolar activities, with the most potent one, IIP0943, demonstrating a potency of 5.1 nM. Featuring a new scaffold of 4-(benzo[*b*]thiophen-7-yloxy)pyrimidine, IIP0943 also exhibits high selectivity for PLK1. It was demonstrated that TransPharmer is a powerful tool for discovery of novel and bioactive ligands.

Introduction

Identifying compounds with bioactivity against desired targets has been one of the important objectives for rational drug discovery. Deep learning-based generative models have emerged as currently predominant methodologies, demonstrating their efficacy in advancing towards this objective[1, 2, 3, 4, 5, 6, 7, 8, 9, 10, 11, 12, 13]. One well-known instance is that scientists at Insilico Medicine successfully employed their generative model, GENTRL, to uncover nanomolar inhibitors for the DDR1 kinase within a short timeline[1]. Beyond GENTRL, researchers exhibit a fervent interest in exploring the potential of molecular generative models through investigations of diverse combinations of model components, including architectures[14, 15, 16, 17, 18, 19], molecular representations[20, 21, 22] and optimization algorithms[23, 24, 25, 26].

Effective as generative models are, their efficiency raises new concerns: how does the creativity of generative models compare to that of humans? Can the designs generated by these models inspire human experts? In 2018, Bush et al. conducted an interesting experiment—a Turing test involving three molecular generators[27], including RG2Smi, a deep learning-based generative model[28]. They found that it was hard for RG2Smi to propose molecular designs that align with those of human medicinal chemists or gain acceptance from them. Moreover, the novelty of the bioactive compounds generated automatically has constantly been under debate[29, 30, 31]. Moret et al. fine-tuned their chemical language models (CLMs) using 46 highly active PI3K γ inhibitors before employing them to generate new inhibitors against PI3K γ kinase. The chemical structures of the most potent ligands designed or inspired by CLMs, namely compounds **18** and **22**, exhibit a high degree of similarity to known PI3K γ inhibitors[2]. Other studies that applied transfer learning to bias molecular generators towards specific protein targets often encounter varying degrees of novelty issues with the bioactive compounds generated[3, 4, 5, 6]. These results underscore the urgent need for a deep understanding of the “correct recipes” for generative models to produce compounds that are bioactive while novel enough, in order to serve as useful copilots for human medicinal chemists.

Pharmacophore-informed generative models present alternative approaches to promote this understanding. The pharmacophore model, rooted in pharmaceutical features, offers a coarse-grained solution for molecular representation, facilitating scaffold hopping among chemically diverse ligands[32, 33]. Furthermore, pharmacophore serves as a bridge linking molecular structure and bioactivity. Given these advantages, there has been a recent surge in interest regarding the utilization of pan-pharmacophore features for molecular generation[34, 35, 36]. For instance, Imrie et al. introduced DEVELOP, a novel pharmacophore-aware generative model employing 3D grids to represent target pharmacophores, for linker design and scaffold elaboration[34]. Their results demonstrated that generative models can leverage pharmacophoric information to produce molecules with novel structures that maintain crucial non-bond interactions with receptors. Similarly, LigDream encodes and decodes 3D voxels representing five common types of pharmacophore features for *de novo* molecular design[35]. Other pan-pharmacophore features have been incorporated into

generative models, including condition vectors indicating the shortest bond distances, as well as the presence, absence, or exact quantities of specific pharmacophoric features[37, 38]. Recently, Zhu et al. introduced PGMG, which employs a fully connected graph containing selected pharmacophore features of a reference compound[39]. PGMG was able to generate drug-like molecules with superior docking scores compared to known bioactive ligands and showcased its capability of scaffold hopping from an initial EGFR inhibitor. However, it is noteworthy that none of the molecules generated by pharmacophore-based generative models have undergone wet lab experimental testing to validate this methodology.

In this study, we present TransPharmer as an innovative pharmacophore-aware generative model, which employs ligand-based pharmacophore kernels to achieve structural abstraction while preserving fine-grained topological information. The ligand-based pharmacophore kernels are similar to those used in the previous studies for ligand-based virtual screening[40, 41]. Our pharmacophore kernels are encoded into multi-scale and interpretable fingerprints, serving as prompts for TransPharmer. The architecture of TransPharmer is reminiscent of a generative pre-training transformer (GPT)[42], as illustrated in Figure 1, establishing a connection between pharmacophores and molecular structures represented by the simplified molecular-input line-entry system (SMILES)[43]. We posit that equipping GPT with pharmacophore knowledge enables the model to focus on the pharmaceutical aspects of the chemical structures and generate drug-like molecules. During our evaluation, TransPharmer demonstrated superior performance compared to other baseline models in tasks involving *de novo* generation and scaffold elaboration under pharmacophoric constraints. We also highlight TransPharmer’s distinct mode in probing the local chemical landscape surrounding a reference compound, rendering it highly suitable for scaffold hopping tasks in drug discovery. We further validate the capability of TransPharmer to produce novel and bioactive ligands through two case studies involving DRD2 and PLK1. Notably, we experimentally tested four generated compounds targeting PLK1, featuring a new series of scaffolds. Among these, three out of four compounds exhibited inhibitory activity below 1 μM , with the most potent one, IIP0943, demonstrating a potency of 5.1 nM (4.8 nM for the reference PLK1 inhibitor). Furthermore, IIP0943 exhibits high selectivity for PLK1 compared to other PLK isoforms. To the best of our knowledge, TransPharmer stands as the first pharmacophore-based generative model successfully executing scaffold hopping to produce novel compounds with potent bioactivity. The 4-(benzo[*b*]thiophen-7-yloxy)pyrimidine scaffold of IIP0943 may offer new insights for obtaining improved PLK1 inhibitors.

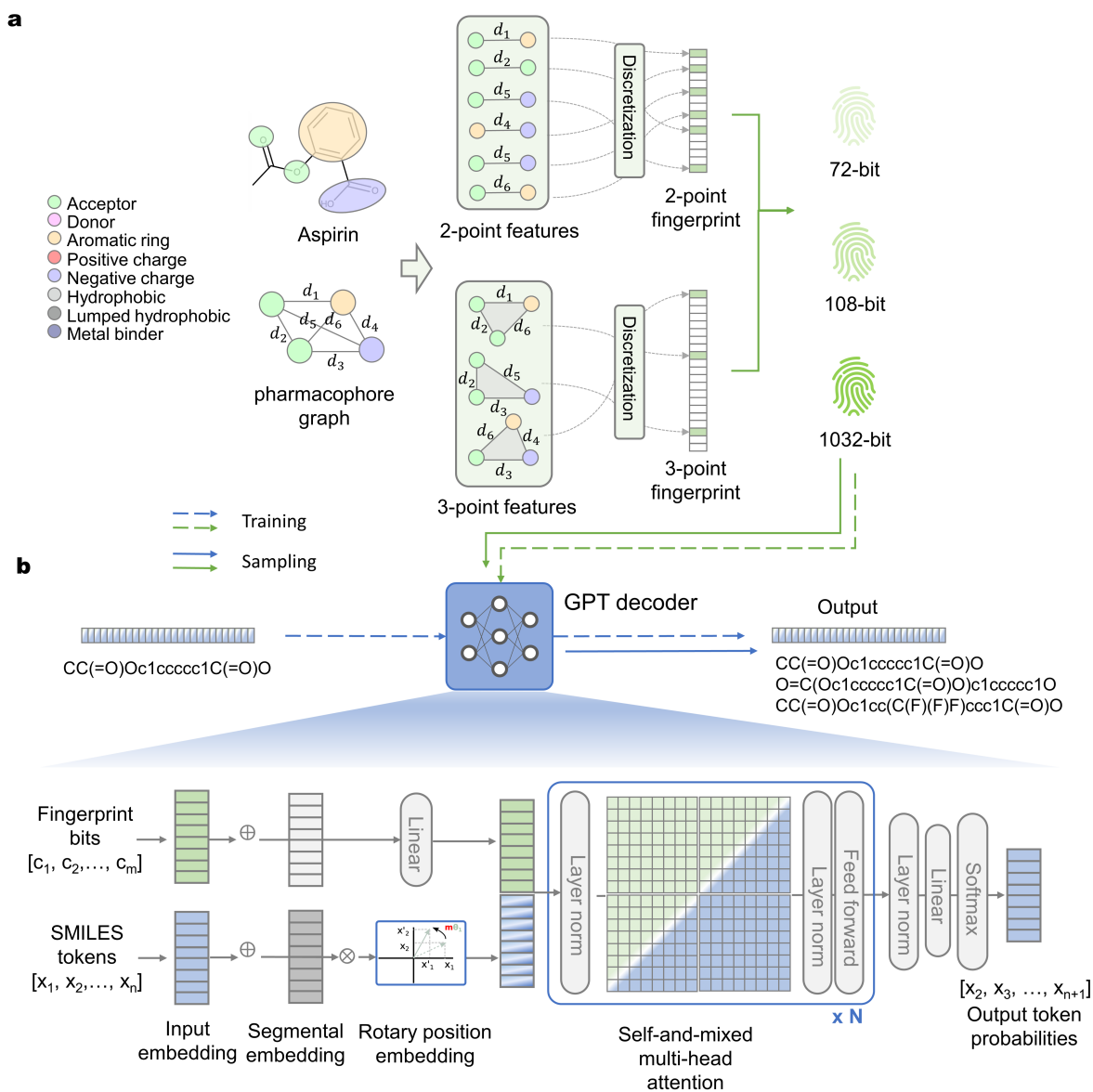


Figure 1: The schematic diagram of TransPharmer architecture. (a) The process of pharmacophore fingerprint extraction. As an example, the chemical structure of Aspirin is converted into a pharmacophoric topology graph with the shortest topological distance between each feature pair computed. All the two-point and three-point pharmacophoric subgraphs are enumerated, and the topological distances are discretized with specific distance bins. 72- and 108-bit pharmacophore fingerprints are constructed from the two-point pharmacophores with different discretization schemes, while 1032-bit pharmacophore fingerprints are the concatenation of fingerprints of two-point and three-point pharmacophores. (b) The architecture of TransPharmer as a pharmacophore fingerprints-driven GPT decoder.

Results

Pharmacophore-constrained molecule generation

One of the central objectives for pharmacophore-conditioned generative models is to generate molecules conforming to the desired pharmacophores, which entails two aspects. Firstly, basic attributes of the pharmacophores of the generated molecules should match those of the target, such as the number of individual pharmacophoric features. Generating molecules with the requisite number of pharmacophoric features has been an essential objective[37, 38, 44]. Here, we computed the averaged difference in the number of individual pharmacophoric features of generated molecules with respect to the target pharmacophores (referred to as D_{count} , see definition in Section "Evaluation metrics"). Secondly, the targeted pharmacophore and the generated molecule’s pharmacophore should have a high degree of overall similarity. Similar to measuring molecular similarity using fingerprints such as Morgan fingerprints[45], pharmacophoric similarity can be calculated by computing the Tanimoto coefficient of two pharmacophoric fingerprints. Here, we adopt ErG fingerprints implemented in RDKit[46] to measure pharmacophoric similarity (referred to as S_{pharma} , see definition in Section "Evaluation metrics") to avoid any artificial positive results of our models. ErG fingerprints are another pharmacophoric fingerprints introduced by researchers in Lilly and have demonstrated potential applications for scaffold hopping[32]. ErG fingerprints show a discernible correlation with the pharmacophoric fingerprints utilized in TransPharmer (Supplementary Figure 1).

We compare our models with LigDream[35], PGMG[39] and DEVELOP[34] as baselines in both tasks of *de novo* generation and scaffold elaboration. As pharmacophoric feature counts have been utilized as explicit controls over the generated molecules[37, 38, 44], we establish another baseline by training a "TransPharmer-count" model that only accepts the requirement of desired amounts of individual features. Furthermore, to investigate the effect of the length of pharmacophoric fingerprints used in our model, three variants of TransPharmer were examined: "TransPharmer-72bit", "TransPharmer-108bit" and "TransPharmer-1032bit". These variants are conditioned on 72-bit, 108-bit, and 1032-bit pharmacophoric fingerprints, respectively.

For the *de novo* generation task (Table 1), TransPharmer models outperform the baseline models by generating molecules with higher pharmacophoric similarity. It is noteworthy that the TransPharmer-count model achieves the lowest deviation in feature counts, while the TransPharmer-1032bit model ranks as the second lowest in this regard. It is not directly comparable between PGMG and other methods since PGMG is primarily designed to align with a specific subset of pharmacophore features (specifically, 3-7 features), whereas models such as TransPharmer aim to generate molecules that satisfy the entire set of pharmacophore features of a reference compound. Consequently, We re-evaluated TransPharmer based on the match score utilized in PGMG and discovered that the match scores achieved by TransPharmer closely approximate

Table 1: Results of the pharmacophore-constrained *de novo* generation task and scaffold elaboration task. The evaluation of LigDream and PGMG only focused on the *de novo* generation task, while DEVELOP was assessed solely on scaffold elaboration, which aligns with their original development purposes. Therefore, n.a. (not applicable) is assigned to the performance of LigDream and PGMG in scaffold elaboration and DEVELOP in *de novo* generation tasks, respectively. Feature count deviation (D_{count}) and pharmacophoric similarity (S_{pharma}) scores were computed with respect to the conditioning compounds. TransPharmer-count refers to the TransPharmer model conditioned on the required number of eight types of pharmacophoric features. TransPharmer-72bit, TransPharmer-108bit and TransPharmer-1032bit refer to the TransPharmer models conditioned on pharmacophoric fingerprints of lengths 72, 108 and 1032, respectively. The numbers in bold indicate the best values.

Method	<i>De Novo</i> Generation		Scaffold Elaboration	
	D_{count}	S_{pharma}	D_{count}	S_{pharma}
LigDream	4.1±2.6	0.47±0.14	n.a.	n.a.
PGMG	9.4±3.7	0.35±0.13	n.a.	n.a.
DEVELOP	n.a.	n.a.	13.0±7.0	0.231±0.160
TransPharmer-count	0.3±0.4	0.48±0.13	0.2±0.3	0.706±0.218
TransPharmer-72bit	4.6±2.6	0.50±0.14	3.0±2.2	0.702±0.176
TransPharmer-108bit	3.6±2.6	0.58±0.15	2.3±1.9	0.751±0.167
TransPharmer-1032bit	3.3±2.0	0.60±0.14	2.1±1.7	0.754±0.166

those of PGMG (Supplementary Table 1). Meanwhile, it is worth noting that PGMG exhibits sensitivity to the parameter of the maximum number of input pharmacophore features specified by users. This sensitivity leads to a notable deviation in molecular sizes compared to the desired targets, particularly when reference compounds possess flexible conformations (Supplementary Table 2).

In the scaffold elaboration task, four TransPharmer models generated molecules with substantially higher pharmacophoric similarity than those of DEVELOP. It seems that DEVELOP exhibits limitations in adhering to the provided pharmacophore conditions, often resulting in the generation of molecules unrelated to and much larger than the reference compound (Supplementary Table 3 and Supplementary Table 4). Among the four TransPharmer models evaluated, the TransPharmer-1032bit model achieves the highest similarity score. The TransPharmer-count model is slightly better than the TransPharmer-72bit model in the mean pharmacophoric similarity, but the variance is larger. The deviation of feature counts is similar to those in the *de novo* generation task.

These findings suggest the benefits of employing pharmacophoric fingerprints that explicitly encode the topology of pharmacophores. In comparison to the 3D voxels of pharmacophoric points encoded by convolutional layers in LigDream or DEVELOP, pharmacophoric fingerprints offer more distinct instructions for molecule generation and may avoid ambiguous guidance resulting from insufficient training of the convolutional neural networks. When compared to simplified condition vectors like feature counts, pharmacophoric fingerprints encompass comprehensive information regarding the topology of pharmacophores, thereby providing superior guidance. In contrast to the use of pharmacophore graphs of selected features in PGMG, TransPharmer exhibits superior control over global molecular properties, such as molecular weight and the

number of heavy atoms, resulting in improved sampling efficiency.

Our analysis also reveals that TransPharmer models with longer pharmacophoric fingerprints consistently generate molecules with higher similarity to the target pharmacophore (Table 1), which conforms to our motivation to obtain fine-grained representations of pharmacophore. Moreover, these models generated molecules that were more similar to the conditioning compound in terms of topological structure and had a relatively higher repetition rate (Supplementary Table 5). Depending on specific needs, the flexibility of TransPharmer allows users to choose which model is most suitable for their intended applications. Overall, the excellent performance and flexibility of TransPharmer make it a viable option for a wide range of scenarios such as novel hits discovery or lead optimization.

Exploring local chemical space

Efficiently exploring the vast chemical space remains a challenging task in drug discovery. One common approach is to start with a few compounds and search their neighborhood but the exploring direction can be quite arbitrary. Molecular similarity-constrained exploration/optimization is one of the widely adopted ways to identify compounds with the desired similarity level to the starting compound[47, 48, 49, 50]. In the previous section, we demonstrated that TransPharmer can efficiently explore the local chemical space in a pharmacophore-constrained fashion. Here, we compare the exploring mode of TransPharmer with those of molecular similarity-constrained methods, using a specific starting compound as a showcase, and illustrate the significance of this exploring mode in drug discovery.

We used Onvansertib, a known inhibitor of PLK1[51], as the starting compound to provide a target pharmacophore. STONED[49], which can perform molecular similarity-constrained exploration by altering the given compound structure, was used for comparison. STONED can rapidly traverse the target neighborhood in the chemical space by mutating the characters of the SELFIES string of the starting compound. Apart from the default setting, STONED can be tuned to produce highly similar structures to the starting compound by restricting the mutation area to the terminal 10% interval of the SELFIES string.[49] STONED in the default and tuned setting are referred to as "STONED" and "STONED-focused", respectively, and the details of each setting can be found in Section "The settings of compared methods". We evaluated five models, including STONED in two settings and three TransPharmer models (72-bit, 108-bit, and 1032-bit), by sampling 10,000 non-duplicate chemical structures and obtaining their pharmacophoric similarity and molecular similarity distributions with respect to the starting compound. The molecular similarity is given by the Tanimoto coefficient of Morgan fingerprints with a radius of 2 implemented by RDKit[46].

Figure 2 shows that the molecular and pharmacophoric similarity scores of the generated molecules from STONED tend to approach the same ends of the scoring range, while those of TransPharmer-72-bit are distributed near the opposite sides (Figure 2b,e). In other words, molecules generated by TransPharmer-

72-bit can be topologically dissimilar but pharmacophorically similar to the starting compound, whereas molecules from STONED are either similar in both molecular structure and pharmacophore to the starting compound, or dissimilar in both aspects (see some examples in Figure 2g). TransPharmer can also produce structurally and pharmacophorically similar structures by using more fine-grained fingerprints (Figure 2c,f).

The plot of the local chemical space spanned by the two similarity axes with the averaged scores of each model marked in the corresponding places in Figure 2 illustrates that TransPharmer and STONED explore the chemical space in different directions and regions (Figure 2d). Molecular similarity constrained methods like STONED traverse along the diagonal, while pharmacophore constrained methods like TransPharmer traverse along a line that is close to horizontal. In addition to providing new directions to explore, TransPharmer models have a unique potential to discover structurally novel molecules while maintaining high pharmacophoric similarity (at the bottom right corner in Figure 2d), which is essential for molecular optimization in practice, such as scaffold hopping.

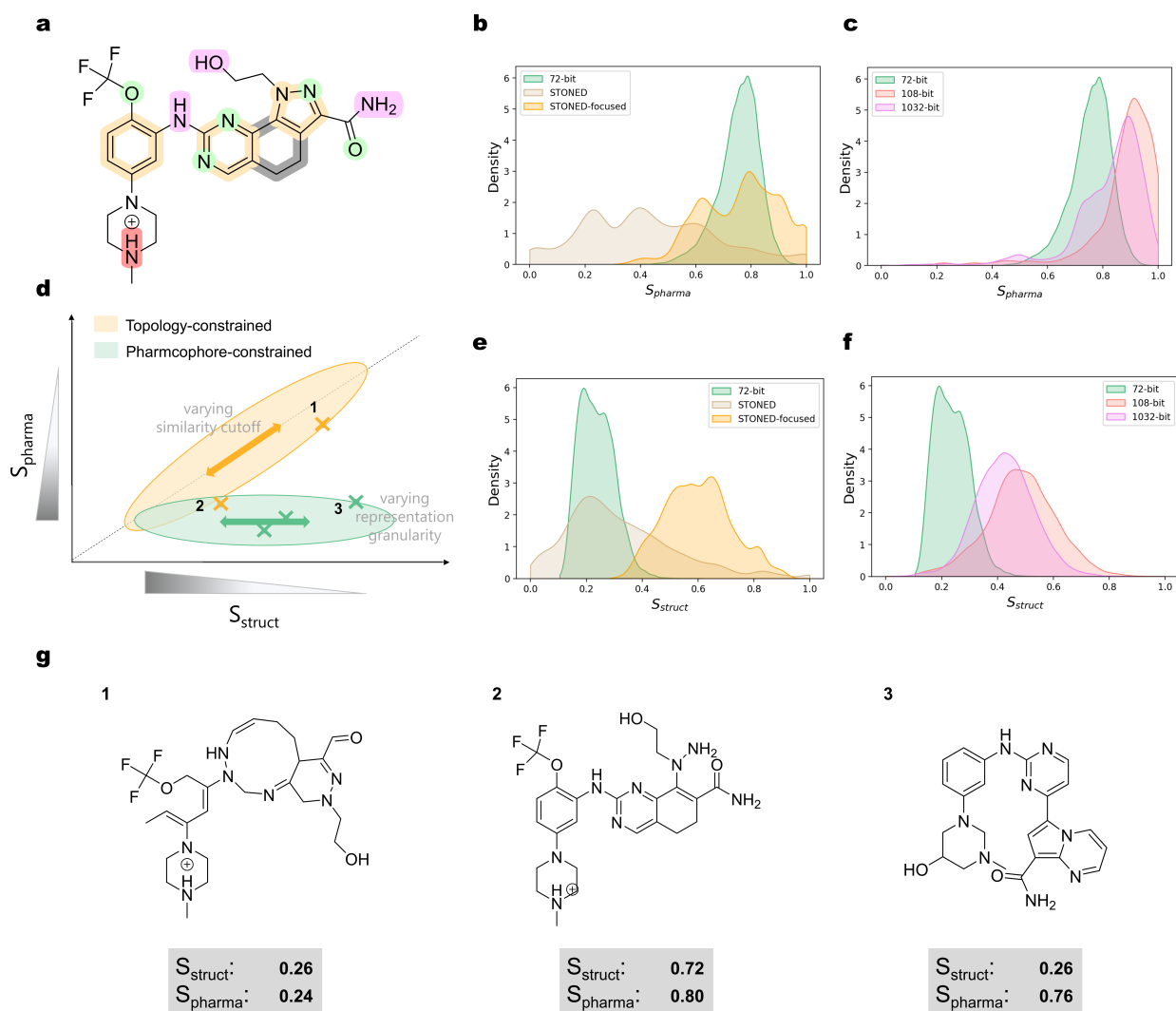


Figure 2: Chemical space exploration around Onvansertib. (a) The 2D chemical structure diagram with pharmacophoric features of Onvansertib. (b) and (e) Distributions comparison of pharmacophoric similarity S_{pharma} and molecular similarity S_{struct} for 72-bit TransPharmer, STONED, and STONED-focused. (c) and (f) Distributions comparison of pharmacophoric similarity S_{pharma} and molecular similarity S_{struct} for 72, 108 and 1032-bit TransPharmer models. (d) A schematic diagram of different exploration modes of pharmacophore- and molecular topology-constrained approaches in the local chemical space spanned by S_{struct} and S_{pharma} . Cross markers label the relative positions of the mean of score distributions for the 5 models in b,c,e,f. Representative samples from area 1, 2 and 3 are shown in (g).

Case study of DRD2

DRD2 is a well-studied target for which many active compounds have been reported. Although ligands with known bioactivities exist, the pursuit of novel ligands with improved characteristics, such as better binding affinity or ADME/T properties, remains ongoing. Therefore, it is essential for generative models to be able to discover active ligands with novel structures, unrestricted by previously observed ligands.

A retrospective experiment was conducted to assess TransPharmer’s ability to discover novel and active ligands. Known DRD2 active ligands were divided into two subsets using scaffold clustering (see Section “Settings for DRD2 recall experiment”), with an average molecular similarity across these subsets of around 0.2. One subset is visible to TransPharmer during training, while the other subset is excluded from the training set. Upon completion of the training, active ligands in the training set were encoded into 72-bit pharmacophoric fingerprints and used by TransPharmer as “active conditions” for molecule generation. The retrieval of the reserved active ligands were examined. This experimental setup mimics a common but challenging scenario in drug discovery to uncover bioactive ligands possessing novel scaffold series given the known active ligands. For comparison, another set of unrelated molecules to DRD2 from the training set were used as “baseline conditions” by TransPharmer (Figure 3b). The comparison between using DRD2 actives as conditions (active conditions) and using baseline conditions aims to demonstrate the difficulty of this task and the consistency of TransPharmer.

The performance of TransPharmer to retrieve active ligands in the reserved subset were evaluated in two aspects. Firstly, the recall rate was calculated for all generated molecules, demonstrating the maximum potential of TransPharmer to discover active ligands under ideal conditions. However, considering the limited budgets for experimental testing in reality, the precision of generative models is also important. In this context, we assessed the (apparent) precision of TransPharmer by enumerating active ligands found within a smaller set of repeatedly generated molecules, specifically 4000 molecules in this experiment. These molecules were generated with a higher sampling probability, indicating a greater confidence for TransPharmer to produce them during the initial sampling phase. The precision is apparent because we only search for known active ligands within the generated set, and the remaining portion likely contains potentially active ligands. Note that 4000 was chosen to be comparable to the number of active ligands unseen by TransPharmer.

Our model rediscovered 4.95% of the active ligands in the unseen subset with sufficient sampling when conditioned on seen active ligands, compared to 0.88% when using baseline conditions. (Figure 3c). If generated molecules highly similar (Tanimoto similarity over 0.8) to any of the active ligands in the unseen subset are considered successful recalls as well, a recall rate of up to 12.1% is observed, consistently higher than that of using baseline conditions (3.2%). (Supplementary Table 6). As for the precision number, up to 15 active ligands in the unseen subset were recalled with a molecular similarity requirement of ≥ 0.8 , which is 7-fold higher than that of using baseline conditions (Supplementary Table 6). Upon inspecting

some recalled active ligands and their most similar counterparts in known active ligands, we observed that in some cases TransPharmer appeared to take shortcuts, such as borrowing subgraphs from seen molecules or making modifications based on them. However, TransPharmer was also able to rediscover truly novel ligands that are structurally distinct from any active ligands it had seen (Figure 3d).

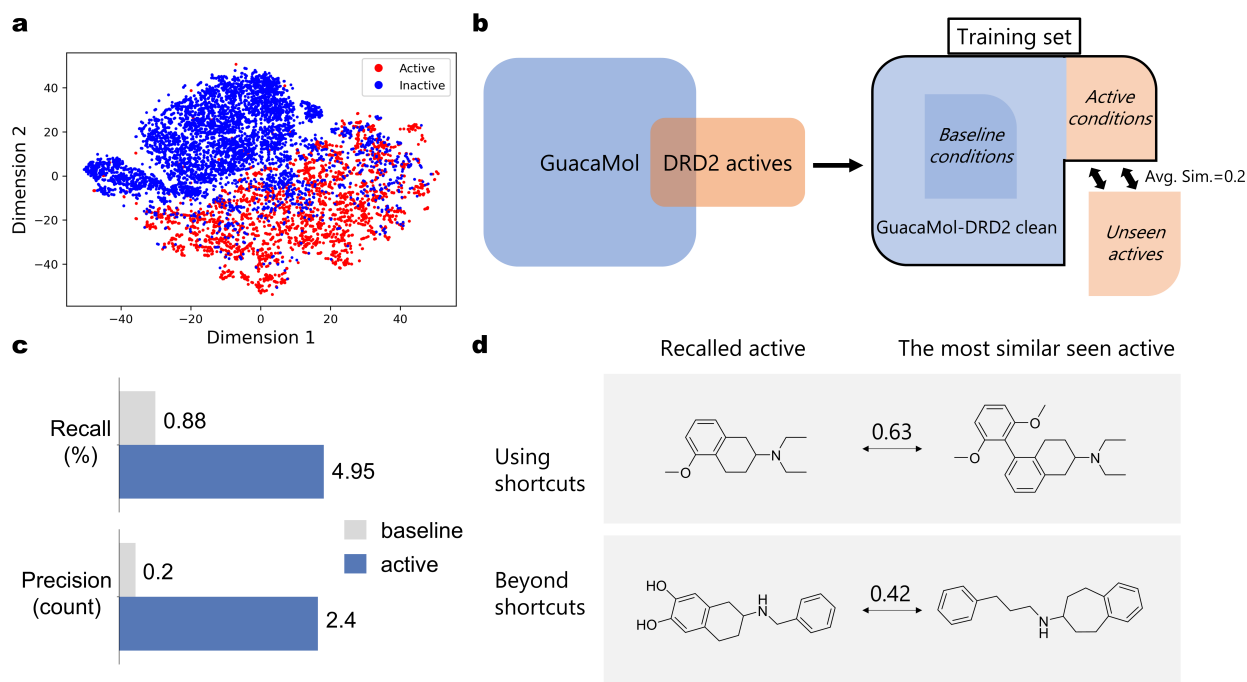


Figure 3: The retrospective experiment for DRD2. a) A t-SNE plot of 108-bit pharmacophore fingerprints of 7939 active and 7939 inactive ligands of DRD2. b) Data preparation in this experiment. “GuacaMol-DRD2 clean” refers to the subset of the original GuacaMol dataset with every known active ligand of DRD2 excluded. Baseline conditions consist of 3717 compounds randomly sampled from “GuacaMol-DRD2 clean”. DRD2 actives were divided into two subsets by scaffold clustering (see Section “Settings for DRD2 recall experiment”). One subset consists of 3717 ligands of DRD2, which are visible to TransPharmer during training and used as active conditions during generation, while the other subset contains 4222 actives to be rediscovered. c) The recall rate and precision count of generated molecules using active and baseline conditions. d) Some recalled active ligands and their most similar counterparts TransPharmer has seen during training. An example of recalling active ligands using shortcuts is shown on the top panel while an example of recalling actives beyond any obvious shortcuts is shown at the bottom panel. The molecular similarity between the recalled and seen ligand is shown.

As previously stated, our search is limited to known active ligands within the generated set and the remaining portion likely contains potentially active ligands. This approach provides a conservative estimate of the proportion of generated molecules that exhibit activity towards DRD2. In order to obtain a more precise estimation, we conducted a virtual screening experiment following the DeepDrugCoder[52]. A DRD2 predictive model was established to predict the probability of a generated molecule exhibiting bioactivity towards DRD2. We then randomly sampled 100 known active compounds from the reserved test set of the

QSAR model. These compounds were used as conditions by TransPharmer to sample 256 times per active compound. The fraction of 25,600 generated SMILES strings that are valid, unique and predicted to be active (with a predicted probability ≥ 0.5) was then computed to compare with the results of DeepDrugCoder. We found that 27% of the generated molecules were predicted as actives, while DeepDrugCoder’s physchem-based (PCB) model reported a fraction of 19% and the fingerprint-based (FPB) model reported 54%. Since the FPB model was trained with the additional information about prior predicted bioactivity from the same QSAR model, the high ratio of molecules predicted to be active is not surprising. On the other hand, our model outperforms the PCB model in terms of ratio by over 40%, emphasizing the importance of using pharmacophoric information to identify active compounds.

Case study of PLK1

PLK1 plays a key role in mitosis progression and has been implicated in various cellular pathways[53, 54, 55, 56, 57]. Targeting PLK1 has emerged as a promising therapeutic strategy for cancer treatment, as the overexpression of PLK1 has been associated with tumor development and progression [58, 59]. In this section, we exemplify the application of TransPharmer in the generation of novel and active PLK1 inhibitors using the topological pharmacophore fingerprint derived from Onvansertib, a potent and selective inhibitor to PLK1 currently undergoing clinical trials (e.g. ClinicalTrials.gov identifier NCT03829410).

One million samples were generated by TransPharmer conditioned on the 72-bit pharmacophore fingerprint of Onvansertib under a low temperature hyperparameter of 0.7. Subsequent to the removal of invalid SMILES strings and duplicated molecules, a total of 178,103 unique molecules were obtained. To gain insights into the chemical space covered by the training set, the generated molecules and the known PLK1 active ligands, a t-distributed stochastic neighbor embedding (t-SNE) plot was generated. As shown in Figure 4a, the generated molecules occupy regions that overlap with those of some, but not all, known ligands, highlighting the directional utilization of PLK1 actives by TransPharmer. The similarity distributions between the generated molecules and Onvansertib also confirm the bias of TransPharmer towards the target pharmacophore, with a median pharmacophoric similarity of 0.92, and demonstrates the capability of TransPharmer to explore novel structures, with a median molecular similarity of 0.28 (Figure 4b).

We then carried out virtual screening against the generated compound library to identify drug-like hit compounds targeting PLK1. First, molecules exhibiting pharmacophoric similarity to Onvansertib below 0.85 were eliminated. Second, adjusted Lipinski’s rule of five[60] with the maximum allowed molecular weight set to 1000 and medicinal chemistry filters[61] were applied to retrieve drug-like generated molecules. Third, molecules containing the same pyrazolo-quinazoline core as Onvansertib were removed. While TransPharmer often produce novel structures, it also tends to generate the identical moieties of the reference compound which best satisfy the conditional pharmacophore fingerprint. The remaining compounds were then docked

into the ATP-binding pocket of PLK1 using Glide in standard precision mode[62]. Polar interaction (hydrogen bonds or salt bridges) between ligands and residue Lys82, Cys133, Glu140 and Asp194 were examined using PLIP[63]. Compounds with a docking score better than -9.0 kcal/mol and forming polar interaction with at least two key residues (where hinge region residue Cys133 is requisite) were kept. These molecules then underwent a two-step clustering process. First, identical Bemis-Murcko scaffolds[64] were grouped; second, the scaffolds were clustered using the Butina algorithm[65], efficiently implemented in chemfp[66], with Morgan fingerprints[45] (radius 2, 2048-bit) as molecular descriptors and a distance threshold of 0.1. 2300 representative members from each cluster with the best docking score and ligand efficiency (docking score divided by molecular weight) were selected and docked into PLK1 again using Glide in extra precision mode[67]. Upon completion of the docking, the molecules were ranked based on their overall performance, considering docking score, ligand efficiency and the binding mode of the No.1 pose.

We systematically inspected the top-ranked generated molecules and selected 42 candidate compounds taking into account factors such as synthesizability, novelty, and the diversity of the generated compounds. The comprehensive listing of the molecular structure for these 42 compounds is available in the Supplementary Information (Supplementary Figure 2 and Supplementary Figure 3). These compounds were classified into five groups based on their core fragments that potentially bind to the hinge region of the kinase domain of PLK1 (Figure 4c). A detailed examination of the known PLK1 inhibitors sharing these cores revealed that the majority of them exhibit low bioactivities, with the exception of ligands featuring core 2, displaying moderate to high bioactivities. Notably, 2/3 (28 out of 42) of our generated compounds carry core 1, whereas only one known active ligands features this core. This underscores the novelty of the new scaffolds containing core 1 as potential PLK1 inhibitors. Subsequently, these 42 compounds underwent binding free energy estimation using MM/GBSA[68, 69, 70, 71] and evaluation of binding stability through 100 ns MD simulation. Among them, four compounds were selected based on their estimated binding free energies and consistent binding behavior within the pocket, of which three compounds carrying core 1 while one compound featuring core 2.

These four compounds, namely lig-3, lig-182, lig-524 and lig-886, were subjected to chemical synthesis. Several minor modifications were made to the generated structures due to the intricacies of chemical synthesis and the need to address potential metabolic instability. The finally synthesized structures largely adhered to the designed structures by TransPharmer (Figure 4d). To clarify, these synthesized structures are referred to as IIP0942, IIP0943, IIP0944 and IIP0945, corresponding to the original lig-3, lig-182, lig-886 and lig-524, respectively. The chemical synthesis route of IIP0943 is shown in Figure 5a; detailed chemical syntheses of all identified compounds are presented in the Supplementary Methods. The synthesis process for IIP0943 starts with the reaction of 3-methoxy-2-nitrobenzaldehyde (**943-0**) and methyl 2-mercaptoacetate to yield **943-1**. Subsequent removal of the methyl group resulted in **943-2**. The reaction of **943-2** with 2,4-dichloro-5-

methylpyrimidine produced **943-3**. The formation of intermediate **B** occurred through a Buchwald–Hartwig amination reaction between 5-bromo-2-methoxyaniline and 1-methylpiperazine. The intermediate **B** was then combined with **943-3** in another Buchwald–Hartwig amination reaction, leading to the formation of ester 943-4. Subsequent treatment with ammonia/methanol resulted in the production of the final compound, IIP0943.

The obtained compounds were then tested for their inhibitory activities against PLK1 kinase. Out of the four tested compounds, three show activities with half maximal inhibitory concentration (IC_{50}) less than 1 μ M (Figure 5b and Supplementary Figure 4). Notably, IIP0943 emerges as the most potent among them, with an IC_{50} value of 5.1 ± 1.7 nM against PLK1, while Onvansertib exhibits an IC_{50} of 4.8 ± 0.7 nM. To investigate the selectivity of these compounds, the IC_{50} values against other PLK isoforms and FAK kinase were determined for the two most potent compounds, namely IIP0943 and IIP0942. The inclusion of FAK kinase was prompted by the identification of a potent FAK inhibitor, BI-4464, which exhibits structural similarity to and forms a comparable binding pose to IIP0943 (PDB ID: 6I8Z). This similarity was revealed during our molecular novelty check, where we searched for analogous compounds to IIP0943 in the ChEMBL database (Section “Molecular novelty check”, Supplementary Figure 5, Supplementary Figure 6 and Supplementary Figure 7). The results indicate that both IIP0942 and IIP0943 exhibit excellent selectivity towards PLK1 within the PLK family (Figure 5c). IIP0943 also shows moderate inhibition against FAK, with an IC_{50} of 264 ± 32 nM, which is over 50-fold less potent than its inhibitory effect against PLK1. IIP0942 also exhibits an IC_{50} of 87.4 ± 11.1 nM against FAK, with an over two-fold selectivity for PLK1.

To understand the potency and selectivity of IIP0943, IIP0943 was docked into the ATP-binding pocket of PLK1. The 4-(benzo[*b*]thiophen-7-yloxy)pyrimidine core of IIP0943 resides between Cys67 and Phe183 (not depicted due to space constraints). The 5-methyl group in the 2-aminopyrimidine is accommodated by a hydrophobic pocket formed by Ala80, Val114 and Leu130 (Figure 6b). Four hydrogen bonds are formed: the 2-aminopyrimidine moiety forms two hydrogen bonds with the backbone NH and C=O groups of the hinge region Cys133; the amide group forms one hydrogen bond with the side chain of Lys82, and another hydrogen bond with Asp194 in the DFG motif. Under physiological conditions, the 4-methylpiperazino moiety becomes protonated, forming a salt bridge with Glu140. This interaction is believed to contribute to the discernible PLK1 selectivity versus PLK 2–3, since the same type of interaction is hampered in both PLK2 and PLK3 where Glu140 is replaced by histidine [72, 73, 51]. The superposition of the docking pose of IIP0943 and the crystal pose of Onvansertib revealed a noteworthy distinction of the orientation of IIP0943’s the benzo[*b*]thiophene-2-carboxamide moiety. This moiety points towards residues in the back cleft from a different angle, which could potentially be compensated by the flexible side chain of Lys82, as indicated in molecular dynamics simulations (data not provided).

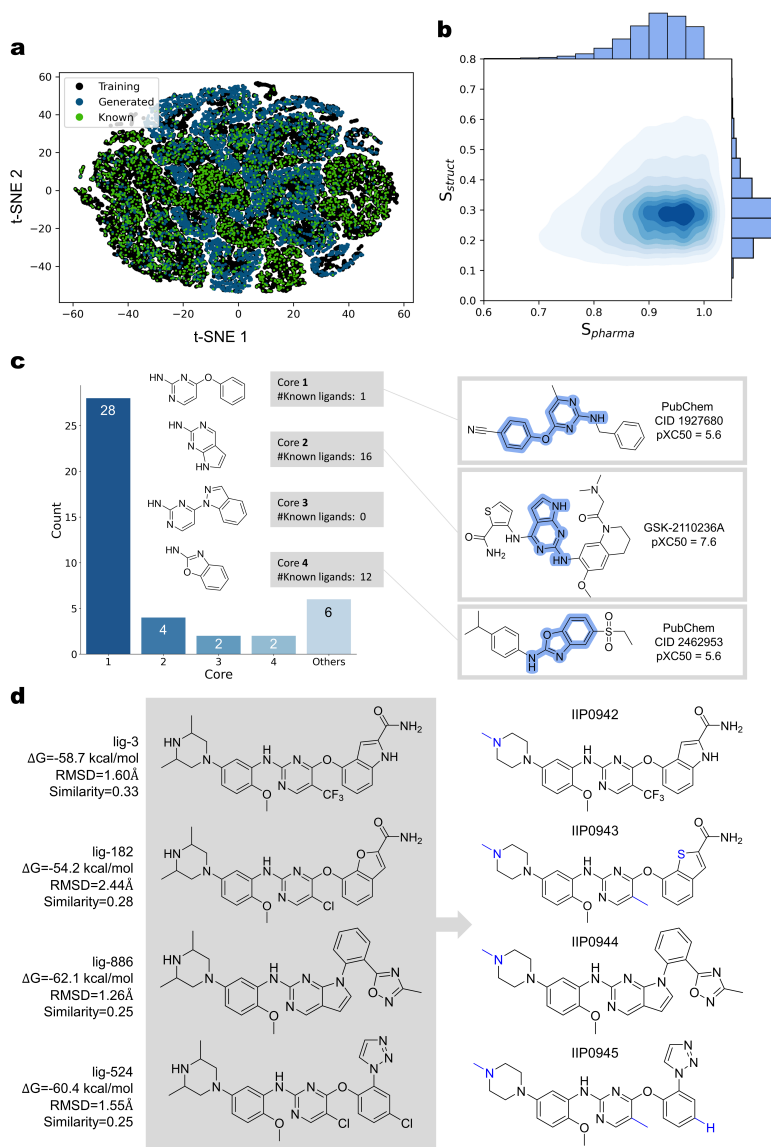


Figure 4: Generation of a virtual compound library against PLK1 using TransPharmer and compound prioritization. (a) Illustration of the chemical space coverage of the generated compounds. T-SNE plots depict the distribution of molecules, with 10,000 randomly selected compounds from the training set, 10,000 from the generated set, and 3,873 representing PLK1 active ligands. (b) Evaluation of pharmacophoric and molecular similarities between the generated compounds and Onvansertib. (c) Categorization of 42 candidate compounds based on the core fragment potentially binding to the hinge region of the active site. Boxes on the right: the most bioactive known PLK1 ligands that carry the substructure of the corresponding category, as well as their bioactivity recorded in uniform expression of “pXC50” in the ExCAPE-DB database (e.g. pXC50=9 corresponds to an IC₅₀ value of 1 nM). The cores are highlighted in blue shade. (d) Comparison of TransPharmer’s designed structures (left) and the synthesized structures with experimental validation (right). Structural modifications are highlighted in blue. The estimated binding free energy, the root-mean-square deviation (RMSD) of binding poses and Morgan similarity scores to Onvansertib are provided for the generated compounds.

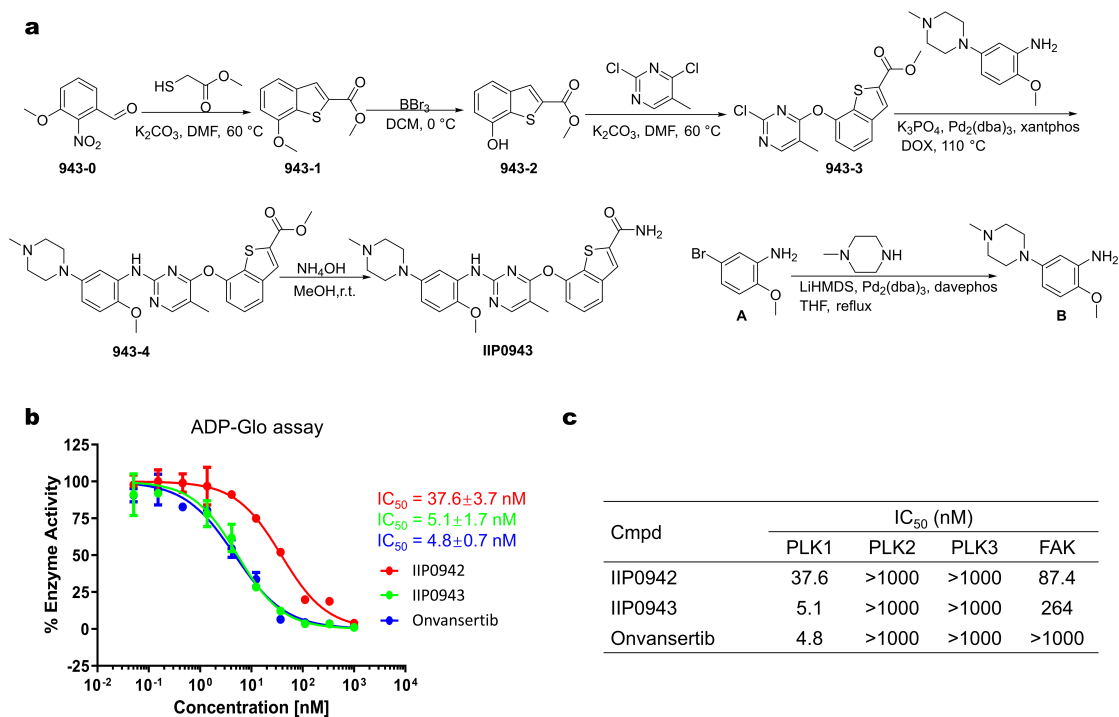


Figure 5: The synthetic route and the enzymatic inhibition activities of the designed compounds. (a) The chemical structure and synthetic route of IIP0943. (b) Dose-activity curves of IIP0942, IIP0943 and Onvansertib in the PLK1 kinase ADP-Glo assays, respectively. Data are presented as mean \pm standard deviation ($n=3$). (c) Enzymatic activity of IIP0942, IIP0943 and Onvansertib against PLK1/2/3 and FAK, respectively.

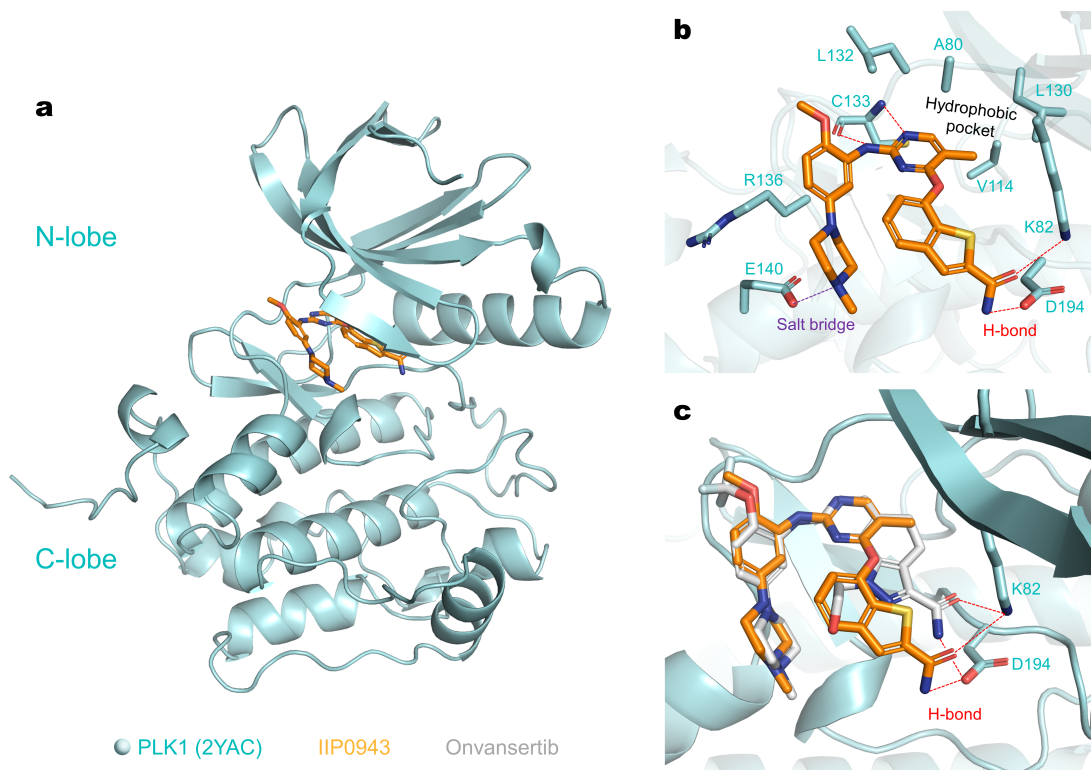


Figure 6: The docking pose of the most potent generated compound, IIP0943. (a) Global view of PLK1 (PDB ID: 2YAC) with the stick model of IIP0943 (in orange) docked into the active site of PLK1. (b) Close-up view of the suggested binding pose of IIP0943 and the interactions between IIP0943 and the PLK1 kinase domain (key residues are shown as pale cyan sticks). (c) Superimposition of IIP0943 (in orange) and the co-crystallized Onvansertib (in gray) in the active site of PLK1. Hydrogen bonds in the back left are shown with dashed red lines.

Discussion

More on chemical space exploration

Yoshimori and colleagues discussed the distinction between structure- and pharmacophore-steered molecular generation in their reinforcement learning-based approach[74]. They compared two agent networks, each guided by rewards based on either molecular similarity or pharmacophoric similarity to a known ligand associated with the target of interest. One notable observation was that the agent guided by the molecular similarity reward successfully generated a larger number of molecules exhibiting topological similarities to the reference ligand, but essentially failed to produce any molecules with a satisfactory pharmacophoric score. This finding implies the inherent limitations of molecular similarity-constrained methods when it comes to exploring the local chemical space.

In our study, we discovered that methods focused on generating structurally analogous compounds could yield molecules that share similarities in both topological structure and ligand pharmacophores. This finding is rational since the concept of ligand pharmacophore is rooted in molecular structure. Moreover, we made an intriguing observation that these two modes of exploration can be complementary, covering distinct regions within the local chemical space. They can also overlap when a fine-grained pharmacophoric representation is employed along with a high molecular similarity cutoff is chosen.

Controllability of TransPharmer

We conducted the three following conditional tests to look at the controllability of our TransPharmer model over conditions: i) set all 72-dim bits to 0; ii) set all 72-dim bits to 1; iii) set one bit to 1 and other bits to 0, traversal to return 72 single-activated-bit fingerprints; Then, we used these fingerprints as condition vectors to generate molecules. The outcomes of conditions i) and ii) were random as expected. The frequency of each bit under each generation condition was then collected for condition iii). The resulted heatmap is shown in Supplementary Figure 8 (top panel), where each row represents the distribution of activation frequency for each bit under the corresponding condition indicated in the horizontal axis of the bottom panel. According to the findings, our model would be well controlled by the single-activated-bit conditions, resulting in enriched molecules that are skewed toward the high-frequency activated bits. The results on low-frequency activated bits showed a random pattern, indicating that the model has the difficulty to learn the low-frequency activated bits, which correspond to relatively rare features, such as positively or negatively charged and zinc-ion-binding moieties, as well as their combinations. This may be alleviated by further fine-tuning with relevant datasets.

On 3D pharmacophores

The complementary nature of protein-ligand interactions as 3D spatial pharmacophores is widely recognized. Ligand-based pharmacophores are analogous to a particular kind of negative image in the binding site. The generated compounds by our model may satiate the actual 3D binding pharmacophores given a predetermined 2D pharmacophore fingerprint. Actually, by listing all potential pharmacophore topologies in the measured Euclidean distances of two or three points, the 3D spatial pharmacophores may be transformed into a variety of 2D pharmacophore topologies. We think that it is doable to manually design a desirable pharmacophore topology. As a result, it is simple to discretize a set of appropriate pharmacophore topologies into bit fingerprints that are numerous criteria to steer molecular generation. Even while ligand-based 3D pharmacophores offer one option to guide the generative model, it is still challenging to guarantee that active ligand conformations are generated. To get around this issue, one might predict active ligand conformations using other deep learning models[75].

Ways to more universal generative models

The pharmacophoric fingerprints used in TransPharmer can be considered as valuable prompts. These prompts enable TransPharmer to seamlessly transition from designing novel ligands for one target to designing for another target, without the need for additional finetuning. This ability was demonstrated in the aforementioned case studies involving DRD2 and PLK1. Consequently, TransPharmer is readily applicable in diverse scenarios.

Compared to other molecular generative models utilizing GPT-like architecture[18], TransPharmer offers dual-fold contributions. Prompted with pharmacophoric fingerprints, TransPharmer incorporate prior knowledge into the generation of pharmaceutically relevant compounds, aligning more effectively with the intentions of medicinal chemists. This paves the way to the establishment of large pharmaceutical generative models that combine multi-modal knowledge in addition to basic chemical rules derived from molecular structures[76]. Another fold of contributions arises from leveraging the structural hopping characteristics of pharmacophores to facilitate the discovery of novel compounds with similar activity against the same pharmaceutical target.

Methods

Pharmacophore features and fingerprint extraction

The molecular graph is first converted into a fully connected graph of pharmacophore features using the definition of ligand-based pharmacophores from RDKit v2021.9 (*BaseFeature.fdef*)[77]. This definition encompasses eight types of pharmacophore features, including hydrogen-bond acceptors and donors, aromatic rings, moieties possessing positive or negative ionizability, hydrophobic entities, or those associated with Zn ion binding. Detailed patterns for each type are presented in the Supplementary Table 7. To derive the pharmacophore fingerprints utilized in TransPharmer, we obtained two-point and three-point combinations of pharmacophore features, as well as the shortest topological distances between each feature pair. The topological distances were discretized into 2-bin (the range for short distances as [0, 3) and for long distances as [3, 8)) or 3-bin (the range for short distances as (0, 2), for medium distances as [2, 5) and for long distances as [5, 8)) signals. When a distance falls within a specific range, the corresponding bit is set to 1, otherwise 0; if the distance exceeds the maximum considered distance, 8 in this study, there will be null signals (00 or 000). For the two-point pharmacophoric features with 2-bin and 3-bin discretization schemes, the lengths of the binary pharmacophore fingerprints obtained are 72 and 108, respectively. For the combination of two- and three-point pharmacophoric features with the 2-bin scheme, the lengths of the fingerprints are 1032. The fingerprint extraction process was built based on the 2D pharmacophore fingerprints modules implemented in RDKit[46].

Model architecture

As illustrated in Figure 1 and Supplementary Figure 9, TransPharmer receives the pairings of a SMILES string and its extracted pharmacophore fingerprint as two-channel input during training. After segmental encoding and positional encoding, these input embeddings are fed into the Transformer decoder with multi-head self-and-mixed attention blocks to decode the SMILES tokens in the next position. The segmental encoding aims to distinguish between tokens and conditions by using explicit label vectors (0s for pharmacophore fingerprint and 1s for SMILES token). The positional encoding adopts a rotary positional encoding[78] by multiplying the embedding vectors by the rotation matrix as follows,

$$Attention(Q, K, V)_m = \frac{\sum_{n=1}^N (R_{\Theta, m}^d \phi(q_m))^T (R_{\Theta, n}^d \varphi(k_n)) v_n}{\sum_{n=1}^N \phi(q_m)^T \varphi(k_n)} \quad (1)$$

where $\varphi(*)$ and $\phi(*)$ are usually non-negative functions, $R_{\Theta, m}^d$ and $R_{\Theta, n}^d$ are rotation matrix. This positional encoding was demonstrated to be more compatible with the linear operation in the attention block and to converge faster during training.[78] A slim version of the GPT-3 model[42] is utilized for the

multi-head Transformer decoder. And self-and-mixed attention blocks adopted for adequate information exchange in order to learn implicit associations. With the processing of the Transformer decoder, the final layer output the probabilities of next SMILES tokens using linear transformation and softmax operations. The hyperparameters of TransPharmer are shown in Supplementary Table 8.

Data set setup

We use the GuacaMol dataset[79], which is derived from the ChEMBL24 database and is composed of about 1.6 million unique compounds. The sizes of the training, validation, and testing sets are 1,273,104 (80%), 79,562 (5%), and 238,681 (15%), respectively, for model development and evaluation, following the data splitting of GuacaMol without further curation. All TransPharmer models in the pharmacophore-constrained molecule generation tasks were trained on the GuacaMol dataset.

A 108-token vocabulary was first constructed from the SMILES strings from the GuacaMol dataset, which contains '#', '%10', '%11', '%12', '(', ')', '-', '1', '2', '3', '4', '5', '6', '7', '8', '9', ':', '=', 'B', 'Br', 'C', 'Cl', 'F', 'I', 'N', 'O', 'P', 'S', '[B-]', '[BH-]', '[BH2-]', '[BH3-]', '[B]', '[Br-]', '[Br+2]', '[C+]', '[C-]', '[CH+]', '[CH-]', '[CH2+]', '[CH2]', '[CH]', '[Cl+]', '[Cl-]', '[Cl+3]', '[Cl+2]', '[F-]', '[F+]', '[H]', '[I+]', '[I+2]', '[I+3]', '[IH2]', '[IH]', '[I-]', '[N+]', '[N-]', '[NH+]', '[NH-]', '[NH2+]', '[NH3+]', '[N]', '[O+]', '[O-]', '[OH+]', '[O]', '[P-]', '[P+]', '[PH+]', '[PH2+]', '[PH]', '[S+]', '[S-]', '[SH+]', '[SH]', '[Se-]', '[Se+]', '[SeH+]', '[SeH]', '[Se]', '[SeH2]', '[Si-]', '[SiH-]', '[SiH2]', '[SiH]', '[Si]', '[SH-]', '[b-]', '[bH-]', '[c+]', '[c-]', '[cH+]', '[cH-]', '[n+]', '[n-]', '[nH+]', '[nH]', '[o+]', '[s+]', '[sH+]', '[se+]', '[se]', 'b', 'c', 'n', 'o', 'p' and 's'. After removing less frequent tokens (including '[Br+2]', '[Br-]', '[Cl+2]', '[Cl+3]', '[Cl+]', '[Cl-]', '[F-]', '[I+2]', '[I+3]', '[I-]', '[P-]', '[SH-]', '[Se-]', '[SeH2]'), a 94-token vocabulary is used to process SMILES strings from different sources. Those contain tokens outside the vocabulary were removed.

8323 DRD2 actives were collected from the ExCAPE-DB[80] and 7939 were left after elimination of invalid SMILES strings (can not parsed by RDKit) and duplicate structures (share the same canonical SMILES strings). Over 40,000 DRD2 inactives were also downloaded from the ExCAPE-DB and 7939 of them were randomly sampled for visualization and comparison with actives. TransPharmer in the recall experiment of DRD2 actives were retrained on the merged dataset of GuacaMol and DRD2 actives, described in Section "Settings for DRD2 recall experiment"

3873 entries of PLK1 actives were also collected from the ExCAPE-DB database and all of them have valid and non-duplicate SMILES strings. Each entry contains the molecular structure in SMILES format and the bioactivity record in uniform expression of "pXC50" (e.g. pIC50 or pEC50. pIC50=9 corresponds to an IC₅₀ value of 1 nM).

Settings for pharmacophore-constrained molecule generation

300 compounds (referred to as conditioning compounds) were randomly selected from the reserved test set, and each model used their pharmacophoric information to guide *de novo* generation of novel molecules. For the task of scaffold elaboration, each conditioning compound is fragmented into two parts by breaking a random acyclic single bond between two non-hydrogen atoms. One fragment of the conditioning compound is chosen arbitrarily as the core or starting fragment, while the other becomes a reference elaboration. Using the core fragments as starting points, each model performs scaffold elaboration guided by the pharmacophoric information of the reference fragments. For both tasks, each model attempts to generate 600 molecules for every conditioning compound, and invalid and duplicate molecules are filtered out before further evaluation. Detailed parameter settings for the three external baseline models can be found in Section "The settings of compared methods".

The settings of compared methods

LigDream[35]. LigDream can generate novel molecules guided by the three-dimensional shape and pharmacophoric features of a reference compound. LigDream contains a shape variational autoencoder (VAE), which encodes a voxelized 3D molecular structure into its latent code and reconstructs the voxelized compound representation from it, and a shape captioning recurrent neural network (RNN), which decodes the voxelized representation to the SMILES of a specific molecule. The LigDream authors found that the VAE reparametrization factor λ and the RNN probabilistic sampling can provide different sources of sampling variability. In this study, we set the reparametrization factor λ to 1.0 and turned off the RNN probabilistic sampling as suggested. The model weight was obtained from their public repository (<https://github.com/compsciencelab/ligdream>).

PGMG[39]. PGMG receives a fully connected graph containing selected pharmacophore features. This graph is encoded using a Gated Graph Convolutional Network to obtain an embedding vector, which is subsequently decoded into SMILES strings using transformer encoder-decoder blocks. In this study, following the training process of PGMG, a pharmacophore hypothesis was constructed by randomly selecting 3-7 pharmacophore features for each test case molecule, and the 3D coordinates for each feature were obtained from the molecular conformation embedded using the ETKDG[81] method, as implemented in RDKit. We utilized the pretrained PGMG (accessible at <https://github.com/CSUBioGroup/PGMG>) to generate 600 samples for each pharmacophore hypothesis. For other exploration settings and evaluation of PGMG, please refer to Table S2 in the supplementary materials.

DEVELOP[34]. DEVELOP integrated pharmacophoric information of the regions to be explored into the process of fragment linking or scaffold elaboration and has shown broad potential in scenarios such as PROTAC design or R-group optimization. We utilized the scripts provided by the authors of DEVELOP

to prepare the pharmacophore information and index files and perform required preprocessing for our testing data. We loaded the pretrained model weights (accessible at <https://github.com/oxpig/DEVELOP>) and adopted the default parameters during generation following the instructions of the setting used to generate molecules with the same number of atoms as the reference molecule.

STONED[49]. Superfast traversal, optimization, novelty, exploration and discovery (STONED) is an algorithm that can perform local chemical subspace exploration around a target molecule and other functionality. STONED achieves these by modifying the SELFIES[21] string representation of the reference molecules. The amount and location of the modified characters have different effects on the similarity between the resultant structures and the original one. Basically, restricting the amount or the location of the SELFIES changes to either the initial or the terminal region yields similar mutated structures[49].

In this study, we utilized this feature of STONED to explore the local chemical space around a target molecule in two different modes. The first one is the default mode (“STONED”) that allows the mutation positions to be chosen randomly and the number of mutations up to 5. The “STONED” mode produces both similar and dissimilar structures to the starting molecule. The second is “STONED-focused” mode that allows only 1 modification and restricts the mutation position to the terminal 10% of the SELFIES. The “STONED-focused” mode was set up intentionally to produce highly similar mutated structures to the target one. For the “STONED” mode, we sampled 10,000 times for each molecule, while for the “STONED-focused” mode we sampled 100,000 times because the mutated structures have a high probability of repeating themselves. Only the non-duplicate parts of the generated molecules were retained by examining their canonical SMILES strings output by RDKit[46].

Evaluation metrics

In this study, we use S_{struct} to represent molecular similarity score which is measured by the Tanimoto coefficient of 2048-bit Morgan circular fingerprints with a radius of 2, and use S_{pharma} to represent pharmacophoric similarity score which is measured by the Tanimoto coefficient of ErG fingerprints[32] implemented by RDKit. Molecules will go through charge neutralization before similarity scoring.

The deviation of pharmacophoric feature counts D_{count} is formulated as follows:

$$D_{count} = \frac{1}{N} \sum_i^N \sum_j^m |n_j^i - n_j^{ref}| \quad (2)$$

where n_j^i is the number of j th pharmacophoric feature in i th generated molecule, n_j^{ref} is the number of j th pharmacophoric feature in the reference molecule, m is the total number of pharmacophoric feature types ($m = 8$ in this study) and N is the total number of generated molecules.

The recall rate in the recall experiment of DRD2 actives is formulated as follows:

$$\text{Recall} = \frac{\#\text{Known actives in the generated set}}{\#\text{Known actives in the reserved set}} \quad (3)$$

The apparent precision is the number of known actives unseen by TransPharmer found within the set of 4000 generated molecules. These molecules were sampled more than once during the generation process and continuously joined the generated set until the size of 4000 was reached.

Settings for DRD2 recall experiment

The Bemis-Murcko scaffolds of the 7939 DRD2 actives were extracted and clustered using Butina algorithm[65] implemented in RDKit[46], with Morgan fingerprints[45] (radius 2, 2048-bit) as molecular descriptors and a distance threshold of 0.4. Then, scaffold clusters were sorted by size in descending order and 3717 ligands with scaffolds in the odd-indexed clusters were added into the training set of TransPharmer, while 4222 ligands with scaffolds in the even-indexed clusters were actives to be recalled. During generation, active ligands in the training set were encoded into 72-bit pharmacophoric fingerprints and used as prompts of TransPharmer to generate 1000 SMILES per condition, yielding a total of 3,717,000 generated samples. 3717 unrelated molecules to DRD2 randomly drawn from the training set (Figure 3b) were also encoded into 72-bit pharmacophoric fingerprints for TransPharmer to generate 1000 SMILES per condition.

DRD2 QSAR model

A classification model employing a Support Vector Machine (SVM) for the prediction of bioactivity was developed following DeepDrugCoder[52]. The standard implementation of SVM from the scikit-learn v0.20.347 Python package was used, with the radial basis function as the kernel function. The model was trained to discriminate active compounds from inactive ones based on their 2,048-bit-radius 2 Morgan fingerprint representations. Model weights and optimized hyperparameters were loaded from <https://github.com/pcko1/Deep-Drug-Coder/tree/master/models>. The model outputs the probability of a compound to be active against DRD2.

t-distributed stochastic neighbor embedding (t-SNE)

To visualize the chemical space encompassed by the generated molecules, the training set and the known PLK1 active ligands, we constructed t-SNE plots. Several important physiochemical parameters associated with drug-like properties were calculated, including molecular weight, the water-octanal partition coefficient[82], the qualitative estimate of drug-likeness[83], the synthetic accessibility score[84], the number of H-bond donors, the number of H-bond acceptors, the number of rotatable bonds and the number of

rings. Employing the Barnes-Hut implementation of the t-SNE algorithm[85], we obtained two-dimensional representations of these parameters for all 3873 PLK1 active ligands and 10000 randomly selected molecules from the training and generated set.

Molecular docking

The receptor structure was taken from the Protein Data Bank (PDB)[86] (PDB ID: 2YAC) and prepared using the Schrodinger Protein Preparation Wizard[87] with default parameters, i.e. we added hydrogens, protonated non-residue molecules at pH 7 ± 2 using Epik[88], removed waters, ions and crystallisation artefacts (e.g. tartaric acid), optimized hydrogen bond assignment at pH 7 using PROPKA[89] and minimized the structure using the OPLS3e force field[90]. A grid was defined using the centroid of the co-crystallised ligand Ovasertib as the centre. Before the docking procedure, the generated ligands were prepared using LigPrep[91] to enumerate unspecified stereocentres, tautomers and protonation states and perform minimization using the OPLS3e force field. Each molecule along with any respective variants were then docked using Glide[62].

Molecular dynamics (MD) simulation

MD simulation was carried out on the systems of PLK1 in complex with generated ligands. The systems were first minimized through steepest descent minimization until the termination condition, i.e. the maximum force below 10.0 kJ/mol, was satisfied. After minimization, the systems were heated to 300 K over 100 picoseconds (ps) using the NVT ensemble with a restraint of 1000 kJ/mol nm⁻² on both the kinase and ligands, followed by an additional 100 ps of NVT equilibration with a restraint solely on the protein. Next, 100 ps of NPT equilibration was conducted. Finally, either a 4-nanosecond (ns) production run for estimating binding free energy or a 100 ns run for evaluating binding stability was conducted. The long-range electrostatics were accounted for by means of the particle mesh Ewald (PME) method, with a cutoff of 12 Å applied uniformly across all the MD simulations. All hydrogen-heavy atom bonds were constrained by the LINCS method, and simulations were executed with a time step of 2 femtoseconds. Temperature coupling utilized the V-rescale method. To assess the stability of the simulated systems, the root-mean-square deviation (RMSD) was computed based on the last 20 ns of the trajectory.

Molecular mechanics with generalised Born and surface area solvation (MM/G-BSA)

The MM/GBSA calculations were conducted employing gmx_MMPBSA v1.6[92], a tool derived from AMBER's MMPBSA.py. The GBOBC2 (igb = 5) model was utilized in this study, with a salt concentration was

set at 0.15 M. For the kinase, the ff14SB force field was employed, while the General Amber Force Field was applied to the generated ligands. Other default parameters for MM/GBSA calculations were applied.

Chemical synthesis

The primary synthetic data are available in the Supplementary Methods.

In vitro kinase activity assays

In vitro kinase activity assays were conducted through ADP-Glo assay services provided by Conrabbio (Conrabbio, China). The protocol for the PLK1 assay is described as follows (protocols for other kinases are very similar). Enzyme, substrate, ATP, and compounds were diluted in a Kinase Buffer composed of 40mM Tris (pH 7.5), 20mM MgCl₂, 0.1mg/ml BSA, and 50μM DTT. In a 384-well low volume plate, 1 μl of the compound or 5% dimethyl sulfoxide (DMSO), 2 μl of PLK1 enzyme (15ng/well), and 2 μl of substrate/ATP mix (final concentration: 20 μM ATP, 0.2μg/μl Casein) were added to each well. The plate was then incubated at 25 °C for 60 minutes to allow for kinase activity. Following the enzymatic reaction, 5 μl of ADP-GloTM Reagent was added to each well, and the plate was incubated at 25 °C for an additional 40 minutes. Subsequently, 10 μl of Kinase Detection Reagent was added, and the plate was incubated for a final 30 minutes at 25 °C. Luminescence was recorded with an integration time of 0.5 seconds.

Molecular novelty check

A molecular novelty check of the designed compounds exhibiting IC₅₀ below 1 μM, namely IIP0942, IIP0943 and IIP0945, was performed within the ExCAPE-DB and ChEMBL databases and using SciFinder. The settings and results can be found in the Supplementary Results.

Code availability

The source codes of TransPharmer have been deposited in the GitLab repository under <http://gitlab.iipharma.cn/zhangjh/transpharmer-repo>.

Data availability

The crystal structure of PLK1 utilized in this study is accessible in the Protein Data Bank (PDB) under the accession code 2YAC. Supplementary data are included with this manuscript. All additional data substantiating the drawn conclusions can be obtained from the authors upon reasonable request.

References

- [1] Zhavoronkov, A. *et al.* Deep learning enables rapid identification of potent ddr1 kinase inhibitors. *Nature biotechnology* **37**, 1038–1040 (2019).
- [2] Moret, M. *et al.* Leveraging molecular structure and bioactivity with chemical language models for de novo drug design. *Nature Communications* **14**, 114 (2023).
- [3] Merk, D., Grisoni, F., Friedrich, L. & Schneider, G. Tuning artificial intelligence on the de novo design of natural-product-inspired retinoid x receptor modulators. *Communications Chemistry* **1**, 68 (2018).
- [4] Grisoni, F. *et al.* Combining generative artificial intelligence and on-chip synthesis for de novo drug design. *Science Advances* **7**, eabg3338 (2021).
- [5] Korshunova, M. *et al.* Generative and reinforcement learning approaches for the automated de novo design of bioactive compounds. *Communications Chemistry* **5**, 129 (2022).
- [6] Li, Y. *et al.* Generative deep learning enables the discovery of a potent and selective ripk1 inhibitor. *Nature Communications* **13**, 6891 (2022).
- [7] Ren, F. *et al.* Alphafold accelerates artificial intelligence powered drug discovery: efficient discovery of a novel cdk20 small molecule inhibitor. *Chemical Science* **14**, 1443–1452 (2023).
- [8] Ballarotto, M. *et al.* De novo design of nurr1 agonists via fragment-augmented generative deep learning in low-data regime. *Journal of Medicinal Chemistry* (2023).
- [9] Chenthamarakshan, V. *et al.* Accelerating drug target inhibitor discovery with a deep generative foundation model. *Science Advances* **9**, eadg7865 (2023).
- [10] Zhu, W. *et al.* Discovery of novel and selective sik2 inhibitors by the application of alphafold structures and generative models. *Bioorganic & Medicinal Chemistry* **91**, 117414 (2023).
- [11] Li, Y. *et al.* Discovery of potent, selective, and orally bioavailable small-molecule inhibitors of cdk8 for the treatment of cancer. *Journal of Medicinal Chemistry* **66**, 5439–5452 (2023).
- [12] Tan, X. *et al.* Automated design and optimization of multitarget schizophrenia drug candidates by deep learning. *European Journal of Medicinal Chemistry* **204**, 112572 (2020).
- [13] Xie, W., Wang, F., Li, Y., Lai, L. & Pei, J. Advances and challenges in de novo drug design using three-dimensional deep generative models. *Journal of Chemical Information and Modeling* **62**, 2269–2279 (2022). URL <http://dx.doi.org/10.1021/acs.jcim.2c00042>.

- [14] Flam-Shepherd, D., Zhu, K. & Aspuru-Guzik, A. Language models can learn complex molecular distributions. *Nature Communications* **13**, 3293 (2022).
- [15] Li, Y. *et al.* DeepScaffold: a comprehensive tool for scaffold-based de novo drug discovery using deep learning. *Journal of chemical information and modeling* **60**, 77–91 (2019).
- [16] Wang, M. *et al.* Relation: A deep generative model for structure-based de novo drug design. *Journal of Medicinal Chemistry* **65**, 9478–9492 (2022).
- [17] Kuznetsov, M. & Polykovskiy, D. Molgrow: A graph normalizing flow for hierarchical molecular generation. In *Proceedings of the AAAI Conference on Artificial Intelligence*, vol. 35, 8226–8234 (2021).
- [18] Bagal, V., Aggarwal, R., Vinod, P. & Priyakumar, U. D. Molgpt: Molecular generation using a transformer-decoder model. *Journal of Chemical Information and Modeling* **62**, 2064–2076 (2021).
- [19] Lee, J. S., Kim, J. & Kim, P. M. Score-based generative modeling for de novo protein design. *Nature Computational Science* 1–11 (2023).
- [20] O’Boyle, N. & Dalke, A. DeepSmiles: an adaptation of smiles for use in machine-learning of chemical structures (2018).
- [21] Krenn, M., Häse, F., Nigam, A. K., Friederich, P. & Aspuru-Guzik, A. Self-referencing embedded strings (selfies): A 100% robust molecular string representation. *Machine Learning: Science and Technology* **1** (2020).
- [22] Zhou, G. *et al.* Uni-mol: a universal 3d molecular representation learning framework (2023).
- [23] Olivecrona, M., Blaschke, T., Engkvist, O. & Chen, H. Molecular de-novo design through deep reinforcement learning. *Journal of cheminformatics* **9**, 1–14 (2017).
- [24] Blaschke, T. *et al.* Reinvent 2.0: an ai tool for de novo drug design. *Journal of chemical information and modeling* **60**, 5918–5922 (2020).
- [25] Wang, J. *et al.* Chemistga: a chemical synthesizable accessible molecular generation algorithm for real-world drug discovery. *Journal of Medicinal Chemistry* **65**, 12482–12496 (2022).
- [26] Li, Y., Pei, J. & Lai, L. Structure-based de novo drug design using 3d deep generative models. *Chemical science* **12**, 13664–13675 (2021).
- [27] Bush, J. T. *et al.* A turing test for molecular generators. *Journal of Medicinal Chemistry* **63**, 11964–11971 (2020).

- [28] Pogány, P., Arad, N., Genway, S. & Pickett, S. D. De novo molecule design by translating from reduced graphs to smiles. *Journal of chemical information and modeling* **59**, 1136–1146 (2018).
- [29] Walters, W. P. & Murcko, M. Assessing the impact of generative ai on medicinal chemistry. *Nature biotechnology* **38**, 143–145 (2020).
- [30] Zhavoronkov, A. & Aspuru-Guzik, A. Reply to ‘assessing the impact of generative ai on medicinal chemistry’. *Nature Biotechnology* **38**, 146–146 (2020).
- [31] Ivanenkov, Y. *et al.* The hitchhiker’s guide to deep learning driven generative chemistry. *ACS Medicinal Chemistry Letters* **14**, 901–915 (2023).
- [32] Stiefl, N., Watson, I. A., Baumann, K. & Zaliani, A. Erg: 2d pharmacophore descriptions for scaffold hopping. *Journal of chemical information and modeling* **46**, 208–220 (2006).
- [33] Reutlinger, M. *et al.* Chemically advanced template search (cats) for scaffold-hopping and prospective target prediction for ‘orphan’ molecules. *Molecular informatics* **32**, 133 (2013).
- [34] Imrie, F., Hadfield, T. E., Bradley, A. R. & Deane, C. M. Deep generative design with 3d pharmacophoric constraints. *Chemical science* **12**, 14577–14589 (2021).
- [35] Skalic, M., Jiménez, J., Sabbadin, D. & De Fabritiis, G. Shape-based generative modeling for de novo drug design. *Journal of chemical information and modeling* **59**, 1205–1214 (2019).
- [36] Skalic, M., Sabbadin, D., Sattarov, B., Sciabola, S. & De Fabritiis, G. From target to drug: generative modeling for the multimodal structure-based ligand design. *Molecular pharmaceutics* **16**, 4282–4291 (2019).
- [37] Yang, Y. *et al.* Syntalinker: automatic fragment linking with deep conditional transformer neural networks. *Chemical science* **11**, 8312–8322 (2020).
- [38] Hadfield, T. E., Imrie, F., Merritt, A., Birchall, K. & Deane, C. M. Incorporating target-specific pharmacophoric information into deep generative models for fragment elaboration. *Journal of Chemical Information and Modeling* **62**, 2280–2292 (2022).
- [39] Zhu, H., Zhou, R., Cao, D., Tang, J. & Li, M. A pharmacophore-guided deep learning approach for bioactive molecular generation. *Nature Communications* **14** (2023). URL <https://doi.org/10.1038/s41467-023-41454-9>.
- [40] Mahé, P., Ralaivola, L., Stoven, V. & Vert, J.-P. The pharmacophore kernel for virtual screening with support vector machines. *Journal of Chemical Information and Modeling* **46**, 2003–2014 (2006).

- [41] Capecchi, A., Probst, D. & Reymond, J.-L. One molecular fingerprint to rule them all: drugs, biomolecules, and the metabolome. *Journal of cheminformatics* **12**, 1–15 (2020).
- [42] Radford, A. & Narasimhan, K. Improving language understanding by generative pre-training (2018).
- [43] Weininger, D. Smiles, a chemical language and information system. 1. introduction to methodology and encoding rules. *Journal of chemical information and computer sciences* **28**, 31–36 (1988).
- [44] Skalic, M., Varela-Rial, A., Jiménez, J., Martínez-Rosell, G. & De Fabritiis, G. Ligvoxel: inpainting binding pockets using 3d-convolutional neural networks. *Bioinformatics* **35**, 243–250 (2019).
- [45] Morgan, H. L. The generation of a unique machine description for chemical structures—a technique developed at chemical abstracts service. *Journal of chemical documentation* **5**, 107–113 (1965).
- [46] Rdkit: Open-source cheminformatics. <https://www.rdkit.org>.
- [47] Jin, W., Barzilay, R. & Jaakkola, T. Junction tree variational autoencoder for molecular graph generation. In *International conference on machine learning*, 2323–2332 (PMLR, 2018).
- [48] Jin, W., Barzilay, R. & Jaakkola, T. Hierarchical generation of molecular graphs using structural motifs. In *International conference on machine learning*, 4839–4848 (PMLR, 2020).
- [49] Nigam, A., Pollice, R., Krenn, M., Gomes, G. D. P. & Aspuru-Guzik, A. Beyond generative models: Superfast traversal, optimization, novelty, exploration and discovery (stoned) algorithm for molecules using selfies. *Chemical Science* **12**, 7079–7090 (2021).
- [50] He, J. *et al.* Transformer-based molecular optimization beyond matched molecular pairs. *Journal of cheminformatics* **14**, 18 (2022).
- [51] Beria, I. *et al.* Nms-p937, a 4,5-dihydro-1h-pyrazolo[4,3-h]quinazoline derivative as potent and selective polo-like kinase 1 inhibitor. *Bioorganic and Medicinal Chemistry Letters* **21**, 2969–2974 (2011).
- [52] Kotsias, P.-C. *et al.* Direct steering of de novo molecular generation with descriptor conditional recurrent neural networks. *Nature Machine Intelligence* **2**, 254–265 (2020).
- [53] Schmucker, S. & Sumara, I. Molecular dynamics of plk1 during mitosis. *Molecular & cellular oncology* **1**, e954507 (2014).
- [54] Luo, J. *et al.* A genome-wide rna screen identifies multiple synthetic lethal interactions with the ras oncogene. *Cell* **137**, 835–848 (2009).
- [55] Yu, C. *et al.* Genome-wide crispr-cas9 knockout screening identifies grb7 as a driver for mek inhibitor resistance in kras mutant colon cancer. *Oncogene* **41**, 191–203 (2022).

- [56] Smits, V. A. *et al.* Polo-like kinase-1 is a target of the dna damage checkpoint. *Nature cell biology* **2**, 672–676 (2000).
- [57] Li, Z. *et al.* Polo-like kinase 1 (plk1) overexpression enhances ionizing radiation-induced cancer formation in mice. *Journal of Biological Chemistry* **292**, 17461–17472 (2017).
- [58] Chiappa, M. *et al.* Present and future perspective on plk1 inhibition in cancer treatment. *Frontiers in Oncology* **12** (2022). URL <https://www.frontiersin.org/articles/10.3389/fonc.2022.903016>.
- [59] Zhang, J., Zhang, L., Wang, J., Ouyang, L. & Wang, Y. Polo-like kinase 1 inhibitors in human cancer therapy: development and therapeutic potential. *Journal of medicinal chemistry* **65**, 10133–10160 (2022).
- [60] Lipinski, C. A., Lombardo, F., Dominy, B. W. & Feeney, P. J. Experimental and computational approaches to estimate solubility and permeability in drug discovery and development settings. *Advanced drug delivery reviews* **23**, 3–25 (1997).
- [61] Polykovskiy, D. *et al.* Molecular sets (moses): a benchmarking platform for molecular generation models. *Frontiers in pharmacology* **11**, 565644 (2020).
- [62] Halgren, T. A. *et al.* Glide: a new approach for rapid, accurate docking and scoring. 2. enrichment factors in database screening. *Journal of medicinal chemistry* **47**, 1750–1759 (2004).
- [63] Salentin, S., Schreiber, S., Haupt, V. J., Adasme, M. F. & Schroeder, M. Plip: fully automated protein–ligand interaction profiler. *Nucleic acids research* **43**, W443–W447 (2015).
- [64] Bemis, G. W. & Murcko, M. A. The properties of known drugs. 1. molecular frameworks. *Journal of medicinal chemistry* **39**, 2887–2893 (1996).
- [65] Butina, D. Unsupervised data base clustering based on daylight’s fingerprint and tanimoto similarity: A fast and automated way to cluster small and large data sets. *Journal of Chemical Information and Computer Sciences* **39**, 747–750 (1999).
- [66] Dalke, A. The chemfp project. *Journal of cheminformatics* **11**, 1–21 (2019).
- [67] Friesner, R. A. *et al.* Extra precision glide: Docking and scoring incorporating a model of hydrophobic enclosure for protein- ligand complexes. *Journal of medicinal chemistry* **49**, 6177–6196 (2006).
- [68] Feig, M. *et al.* Performance comparison of generalized born and poisson methods in the calculation of electrostatic solvation energies for protein structures. *Journal of computational chemistry* **25**, 265–284 (2004).

- [69] Onufriev, A., Case, D. A. & Bashford, D. Effective born radii in the generalized born approximation: the importance of being perfect. *Journal of computational chemistry* **23**, 1297–1304 (2002).
- [70] Bashford, D. & Case, D. A. Generalized born models of macromolecular solvation effects. *Annual review of physical chemistry* **51**, 129–152 (2000).
- [71] Onufriev, A., Bashford, D. & Case, D. A. Modification of the generalized born model suitable for macromolecules. *The Journal of Physical Chemistry B* **104**, 3712–3720 (2000).
- [72] Emmitte, K. A. *et al.* Design of potent thiophene inhibitors of polo-like kinase 1 with improved solubility and reduced protein binding. *Bioorganic & medicinal chemistry letters* **19**, 1694–1697 (2009).
- [73] Beria, I. *et al.* Identification of 4, 5-dihydro-1 h-pyrazolo [4, 3-h] quinazoline derivatives as a new class of orally and selective polo-like kinase 1 inhibitors. *Journal of medicinal chemistry* **53**, 3532–3551 (2010).
- [74] Yoshimori, A., Kawasaki, E., Kanai, C. & Tasaka, T. Strategies for design of molecular structures with a desired pharmacophore using deep reinforcement learning. *Chemical and Pharmaceutical Bulletin* **68**, 227–233 (2020).
- [75] Stärk, H., Ganea, O., Pattanaik, L., Barzilay, R. & Jaakkola, T. Equibind: Geometric deep learning for drug binding structure prediction. In *International Conference on Machine Learning*, 20503–20521 (PMLR, 2022).
- [76] Fang, Y. *et al.* Knowledge graph-enhanced molecular contrastive learning with functional prompt. *Nature Machine Intelligence* 1–12 (2023).
- [77] Landrum, G. A., Penzotti, J. E. & Putta, S. Feature-map vectors: a new class of informative descriptors for computational drug discovery. *Journal of computer-aided molecular design* **20**, 751–762 (2006).
- [78] Su, J., Lu, Y., Pan, S., Wen, B. & Liu, Y. Roformer: Enhanced transformer with rotary position embedding. *arXiv preprint arXiv:2104.09864* (2021).
- [79] Brown, N., Fiscato, M., Segler, M. H. & Vaucher, A. C. Guacamol: Benchmarking models for de novo molecular design. *Journal of Chemical Information and Modeling* **59**, 1096–1108 (2019). URL <https://doi.org/10.1021/acs.jcim.8b00839>. PMID: 30887799, <https://doi.org/10.1021/acs.jcim.8b00839>.
- [80] Sun, J. *et al.* Escape-db: an integrated large scale dataset facilitating big data analysis in chemogenomics. *Journal of cheminformatics* **9**, 1–9 (2017).
- [81] Riniker, S. & Landrum, G. A. Better informed distance geometry: using what we know to improve conformation generation. *Journal of chemical information and modeling* **55**, 2562–2574 (2015).

- [82] Wildman, S. A. & Crippen, G. M. Prediction of physicochemical parameters by atomic contributions. *Journal of chemical information and computer sciences* **39**, 868–873 (1999).
- [83] Bickerton, G. R., Paolini, G. V., Besnard, J., Muresan, S. & Hopkins, A. L. Quantifying the chemical beauty of drugs. *Nature chemistry* **4**, 90–98 (2012).
- [84] Ertl, P. & Schuffenhauer, A. Estimation of synthetic accessibility score of drug-like molecules based on molecular complexity and fragment contributions. *Journal of cheminformatics* **1**, 1–11 (2009).
- [85] Van Der Maaten, L. Accelerating t-sne using tree-based algorithms. *The journal of machine learning research* **15**, 3221–3245 (2014).
- [86] Berman, H. M. *et al.* The Protein Data Bank. *Nucleic Acids Research* **28**, 235–242 (2000). URL <https://doi.org/10.1093/nar/28.1.235>. <https://academic.oup.com/nar/article-pdf/28/1/235/9895144/280235.pdf>.
- [87] Madhavi Sastry, G., Adzhigirey, M., Day, T., Annabhimoju, R. & Sherman, W. Protein and ligand preparation: parameters, protocols, and influence on virtual screening enrichments. *Journal of computer-aided molecular design* **27**, 221–234 (2013).
- [88] Shelley, J. C. *et al.* Epik: a software program for pk a prediction and protonation state generation for drug-like molecules. *Journal of computer-aided molecular design* **21**, 681–691 (2007).
- [89] Søndergaard, C. R., Olsson, M. H., Rostkowski, M. & Jensen, J. H. Improved treatment of ligands and coupling effects in empirical calculation and rationalization of p k a values. *Journal of chemical theory and computation* **7**, 2284–2295 (2011).
- [90] Roos, K. *et al.* Opls3e: Extending force field coverage for drug-like small molecules. *Journal of chemical theory and computation* **15**, 1863–1874 (2019).
- [91] Schrödinger, LLC, New York, NY. Ligprep.
- [92] Valdés-Tresanco, M. S., Valdés-Tresanco, M. E., Valiente, P. A. & Moreno, E. gmx_mmpbsa: a new tool to perform end-state free energy calculations with gromacs. *Journal of chemical theory and computation* **17**, 6281–6291 (2021).

End Notes

Acknowledgements

This work was supported in part by the National Natural Science Foundation of China (grants 22033001 and 21673010) and the Chinese Academy of Medical Sciences (grant 2021-I2M-5-014).

Author Contributions

Y. X. devised the ideas. J. Z. and W. X. implemented the deep learning model and performed the model training. W. X., J. Z. and Y. X. discussed and analysed the data. W. X., Q. X. and C. G. conducted the compound screening and prioritization. Y. X. and L. L. and J. P. supervised the project. W. X., J. Z., Y. X., L. L. and J. P. wrote the manuscript.

Declaration of Interests

The authors declare no competing interests.